SCIENCE CHINA Materials ARTICLES

mater.scichina.com link.springer.com Published online 14 May 2021 | https://doi.org/10.1007/s40843-020-1651-5

Structural optimization of acceptor molecules guided by a semi-empirical model for organic solar cells with efficiency over 15%

Lingxian Meng[1†], Huan-Huan Gao[1†], Simin Wu[1†], Yanna Sun[1], Xiangjian Wan[1], Yang Yang[2], Jian Wang[2], Ziqi Guo[1], Hongbin Chen[1], Chenxi Li[1] and Yongsheng Chen[1*]

ABSTRACT Despite much progress in organic solar cells (OSCs), higher efficiency is still the most desirable goal and can indeed be obtained through rational design of active layer materials and device optimization according to the theoretical prediction. Herein, under the guidance of a semi-empirical model, two new non-fullerene small molecule acceptors (NF-SMAs) with an acceptor-donor-acceptor (A-D-A) architecture, namely, 6T-OFIC and 5T-OFIC, have been designed and synthesized. 6T-OFIC exhibits wider absorption spectrum and a red-shifted absorption onset (λ_{onset}) of 946 nm due to its extended conjugation central unit. In contrast, 5T-OFIC with five-thiophene-fused backbone has an absorption with the λ_{onset} of 927 nm, which is closer to the predicted absorption range for the best single junction cells based on the semi-empirical model. Consequently, the device based on 5T-OFIC yields a higher power conversion efficiency (PCE) of 13.43% compared with 12.35% of the 6T-OFIC-based device. Furthermore, an impressive PCE of 15.45% was achieved for the 5T-OFIC-based device when using F-2Cl as the third component. 5T-OFIC offers one of a few acceptor cases with efficiencies over 15% other than Y6 derivatives.

Keywords: organic solar cells, acceptor-donor-acceptor (A-D-A), semi-empirical model, non-fullerene acceptor, high efficiency

INTRODUCTION

Organic solar cells (OSCs) have received intense research interest and great progress in recent years [1–17]. Compared with inorganic silicon-based solar cells, OSCs show the merits of low cost, mechanical flexibility, light weight, and roll-to-roll production [1,8,18–20]. Most recently, nonfullerene small-molecule acceptors (NF-SMAs), especially those with the acceptor-donor-acceptor (A-D-A) architecture, have attracted much attention and achieved impressive power conversion efficiencies (PCEs) of 16%–18% [12,21–33]. Despite significant progress, OSCs still fall behind in performance compared with inorganic photovoltaics. Higher efficiency is still highly desirable and can be indeed obtained according to the theoretical prediction [8–10]. Recently, a semi-empirical model was proposed to screen the active materials and a record PCE of 17.36% was achieved for the tandem solar cell [10]. In fact, the model can be extended to guide the design of active layer materials for single-junction cells [15,34]. For example, PCEs of ~20% can be achieved from the model, if the absorption onset (λ_{onset}) is around 880–930 nm with an average external quantum efficiency (EQE) of 80%, an fill factor (FF) of 80%, and an energy loss (E_{loss}) of 0.45 eV, i.e., open-circuit voltage (V_{oc}) of 0.90–0.96 V, and short-circuit current density (J_{sc}) of 26.00–27.99 mA cm^{-2}. To this end, the λ_{onset} around 880–930 nm should be the first thing to be considered for the design of new active layer materials, since the wide and efficient absorption of sunlight is the starting point for any efficient solar cell. Moreover, other parameters, such as FF, EQE, and E_{loss} are directly related to the device fabrication and optimization [8,9,14].

In our previous work, we reported an A-D-A type non-fullerene acceptor (NFA) 4TIC with the λ_{onset} of 900 nm, and an optimized PCE of 10.87% was obtained with a V_{oc}

[1] The Centre of Nanoscale Science and Technology and Key Laboratory of Functional Polymer Materials, Institute of Polymer Chemistry, State Key Laboratory of Elemento-Organic Chemistry, College of Chemistry, Renewable Energy Conversion and Storage Center (RECAST), Nankai University, Tianjin 300071, China
[2] The Institute of Seawater Desalination and Multipurpose Utilization, Ministry of Natural Resources (Tianjin), Tianjin 300192, China
† These authors contributed equally to this paper.
* Corresponding author (email: yschen99@nankai.edu.cn)

of 0.80 V, a J_{sc} of 20.58 mA cm^{-2} and an FF of 0.66 [35]. Although the λ_{onset} of the 4TIC has reached 900 nm, the J_{sc} is much lower than the ideal value, presumably ascribed to the unfavorable active layers. Then, in order to improve J_{sc}, recently, we reported two A-D-A acceptors, 3TT-ClC and 3TT-OClC, using a six-thiophene-fused (6T) molecule as the backbone and a stronger electron-withdrawing (5,6-dichloro-3-oxo-2,3-dihydro-1*H*-indene-2,1-diylidene) dimalononitrile (INCN-2Cl) unit as the terminal group. Compared with 3TT-ClC, 3TT-OClC with the introduction of alkyl chains on the backbone exhibited a high efficiency over 13% [36]. But based on the semi-empirical model, the device performance of 3TT-OClC is limited by its over redshifted absorption with an absorption onset of 946 nm. Thus, we thought it might be possible to achieve higher device performance if the absorption onset can be tuned down to around 880–930 nm through optimization of the molecular backbone and terminal groups.

Regarding these, herein, we designed and synthesized two A-D-A acceptors, 6T-OFIC and 5T-OFIC with six- (6T) and five-thiophene-fused (5T) central cores, respectively. Meanwhile, INCN-2F was used as the terminal group, which proved to be slightly blue-shifted than INCN-2Cl as used in 3TT-OClC. The optimal PM6:5T-OFIC-based device exhibited a much higher PCE of 13.43% compared with 12.35% of the PM6:6T-OFIC-based device. Furthermore, by using F-2Cl as the third component, the ternary OSCs based on 5T-OFIC obtained an outstanding PCE of 15.45%, which offers one of the very few cases with efficiencies over 15% other than Y6 derivatives. These results indicate that high-performance devices can be achieved through molecular design following the semi-empirical model.

RESULTS AND DISCUSSION

Synthesis and characterization

The synthetic routes of 6T-OFIC and 5T-OFIC are shown in Scheme 1, and the detailed synthetic processes including characterization data are displayed in the Supplementary information. 6T-OFIC was synthesized by the Knoevenagel condensation between 6T-O-2CHO and INCN-2F, in which the 6T-O-2CHO was prepared according to the literature procedure [36]. For 5T-OFIC, compound 3 was obtained through the two-step Stille coupling reaction. Then, the nucleophilic substitution reaction between compound 3 and excess aryl lithium reagents could get the tertiary alcohol intermediate, which was used without further purification for the next step directly to afford the central asymmetric intermediate 5T-O using concentrated H_2SO_4 in tetrahydrofuran. The dialdehyde precursor 5T-O-2CHO was prepared by the Vilsmeier–Haack reaction from 5T-O. The desired acceptor 5T-OFIC was obtained by the Knoevenagel condensation with a high yield. As shown in Fig. S1, the thermal stability of the two molecules was investigated by the thermogravimetric analysis (TGA). Both of them show high thermal stability and the decomposition temperatures at 5% weight loss are 348 and 325°C for 6T-OFIC and 5T-OFIC, respectively.

The optical absorption properties of 6T-OFIC and 5T-OFIC in dilute chloroform and thin films were studied and shown in Fig. 1 and Table 1. The two acceptors in solution show very similar intense absorption in the range of 700–850 nm. But compared with 6T-OFIC, 5T-OFIC shows slightly blue-shift in solution, which is mainly due to the shortened backbone conjugation length. Compared with the solution state, the two molecules exhibit obvious red-shifts (~45 nm) in their solid state, demonstrating well intermolecular π-π stacking in the solid state. The optical bandgaps (E_g^{opt}) of 6T-OFIC and 5T-OFIC calculated from their thin-film absorption edges are 1.31 and 1.34 eV, corresponding to the λ_{onset} of 946 and 927 nm, respectively. Obviously, the absorption edge of 5T-OFIC is in the range of 880–930 nm, which is more suitable for single-junction device according to our semi-empirical analysis. A similar result was obtained from the electrochemical study. The energy levels of the two molecules were investigated by electrochemical cyclic voltammetry (CV) (Fig. S2). Based on the oxidation and reduction onsets, the highest occupied molecular orbital (HOMO) level and the lowest unoccupied molecular orbit (LUMO) energy levels were estimated to be −5.47 and −3.89 eV for 6T-OFIC, −5.51 and −3.86 eV for 5T-OFIC (Fig. 2c), respectively. The lower HOMO level of 5T-OFIC indicates that this molecular strategy indeed broadens the bandgap of 6T-OFIC, which is in accordance with the measured optical bandgaps.

Device structure and photovoltaic properties

To evaluate the potential photovoltaic performance of 6T-OFIC and 5T-OFIC, solution-processed OSCs were fabricated using an inverted device structure of indium tin oxide (ITO)/ZnO/poly[(9,9-bis(3'-((*N*,*N*-dimethyl)-*N*-ethylammonium)-propyl)-2,7-fluorene)-alt-2,7-(9,9-dioctylfluorene)]dibromide (PFN-Br)/active layers/MoO_x/Ag (Fig. 2b). For complementary absorption and matched energy level, polymer donor PM6 was selected as the donor material (Fig. 2a) [37]. After a series of optimiza-

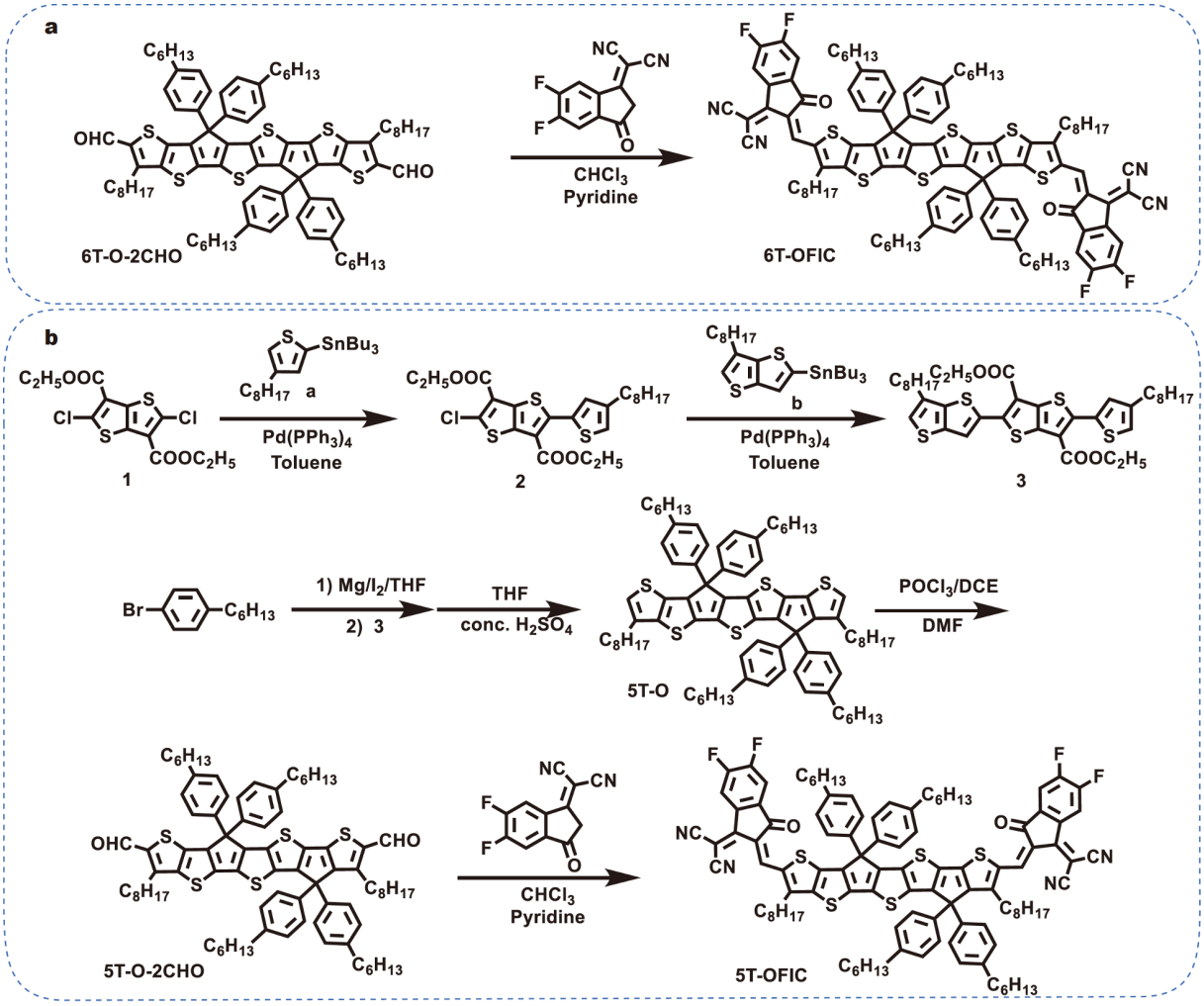

Scheme 1 The synthetic routes of (a) 6T-OFIC and (b) 5T-OFIC.

tion, the optimal PM6:6T-OFIC-based device achieves a PCE of 12.35% with a V_{oc} of 0.782 V, a J_{sc} of 22.69 mA cm^{-2}, and an FF of 0.696, while the optimal PM6:5T-OFIC-based device achieves a higher PCE of 13.43% with a V_{oc} of 0.794 V, a J_{sc} of 24.84 mA cm^{-2}, and an FF of 0.681. The histograms of the PCE counts for 10 individual devices at optimized conditions are shown in Fig. S3. Besides, small energy losses of 0.594 eV for the 6T-OFIC-based device and 0.601 eV for the 5T-OFIC-based device were obtained, which were mainly ascribed to the lower radiative energy losses (ΔE_2) and non-radiative energy losses (ΔE_3), as shown in Fig. S4 and Table S1.

The EQE spectra of the two devices are shown in Fig. 2e. Though the 6T-OFIC-based device shows a much wider EQE responding range than the 5T-OFIC-based device, the 5T-OFIC-based device shows a stronger photo response from 300 to 930 nm with EQE values over 70% (500–850 nm), indicating the efficient photon harvesting and charge collection, and resulting in the higher J_{sc}. The integrated photocurrents of PM6:6T-OFIC and PM6:5T-OFIC from EQE spectra are 22.29 and 24.49 mA cm^{-2}, respectively, which agrees well with the J_{sc} values obtained from the corresponding *J-V* curves (Fig. 2d and Table 2 and Tables S2, S3).

To understand the charge generation and dissociation behavior in the two OSCs, the plots of photocurrent density (J_{ph}) *versus* effective voltage (V_{eff}) were measured. Herein, $J_{ph} = J_L - J_D$, where J_L and J_D are the current densities under illumination and in the dark, respectively, and $V_{eff} = V_0 - V_a$, where V_a is the applied voltage and V_0 is the voltage at $J_{ph} = 0$ [38]. As shown in Fig. 3a, the devices

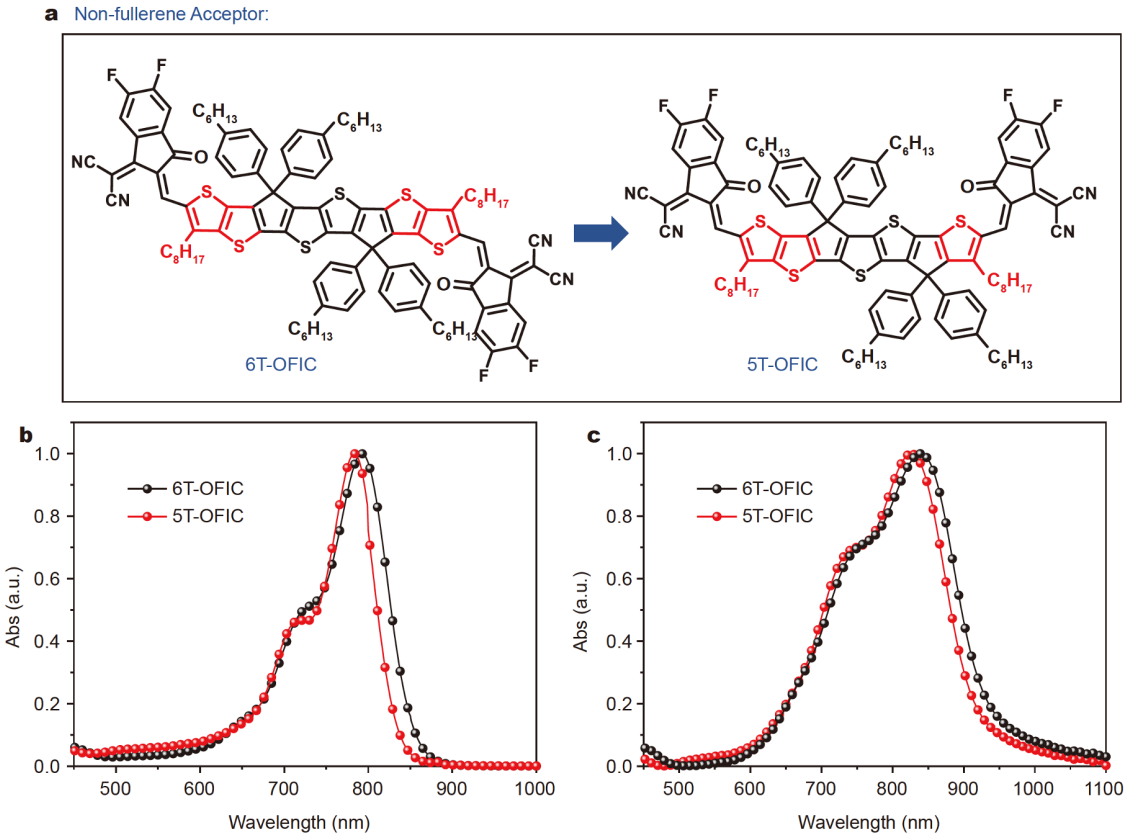

Figure 1 (a) Chemical structures of 6T-OFIC and 5T-OFIC. (b, c) UV-vis absorption spectra of 6T-OFIC and 5T-OFIC in (b) chloroform solution and (c) thin film.

Table 1 The optical and electrochemical properties of 6T-OFIC and 5T-OFIC

Comp.	λ_{max}^{CF} (nm)	λ_{max}^{film}(nm)	HOMO (eV)	LUMO (eV)	λ_{onset}^{film} (nm)	E_g^{opt} (eV)
6T-OFIC	792	839	−5.47	−3.89	946	1.31
5T-OFIC	784	826	−5.51	−3.86	927	1.34

all reach saturation (J_{sat}) when V_{eff} reaches ~1.5 V, indicating charge recombination is minimized at higher voltages. The charge dissociation and collection probability can be estimated from the ratio of J_{ph}/J_{sat}. Under the short-circuit conditions, the J_{ph}/J_{sat} values are 93.2% and 94.5% for the 6T-OFIC-based and 5T-OFIC-based devices, respectively. Under maximal power output conditions, the values of J_{ph}/J_{sat} are 79.3% and 80.9% for the 6T-OFIC-based and 5T-OFIC-based devices, respectively. The higher value of the 5T-OFIC-based device suggests its more efficient exciton dissociation and higher charge transport efficiency. The light-intensity dependence of J_{sc} was also measured to further investigate the relationship between charge recombination and transport in the photoactive layer. As presented in Fig. 3b, recombination parameters obtained by the equation of $J_{sc} \propto P^{\alpha}$, with the exponent α are 0.95 for PM6:6T-OFIC and 0.98 of PM6:5T-OFIC, respectively, indicating that bimolecular recombination is effectively suppressed, especially for the 5T-OFIC-based device, supporting their high FF. The dependence of V_{oc} on light intensity was also estimated to obtain a deeper understanding of the recombination process. As shown in Fig. S5, the PM6:6T-OFIC- and PM6:5T-OFIC-based devices show slops of $1.13kT/q$ and $1.05kT/q$, respectively, where k is the Boltzmann constant, T is the temperature in Kelvin, and q is the elementary charge. The slope close to kT/q generally indicates smaller amounts of trap-assisted recombination, and these results demonstrate weaker trap-assisted recombination losses in the PM6:5T-OFIC-based devices. Fig. 3c, d show the

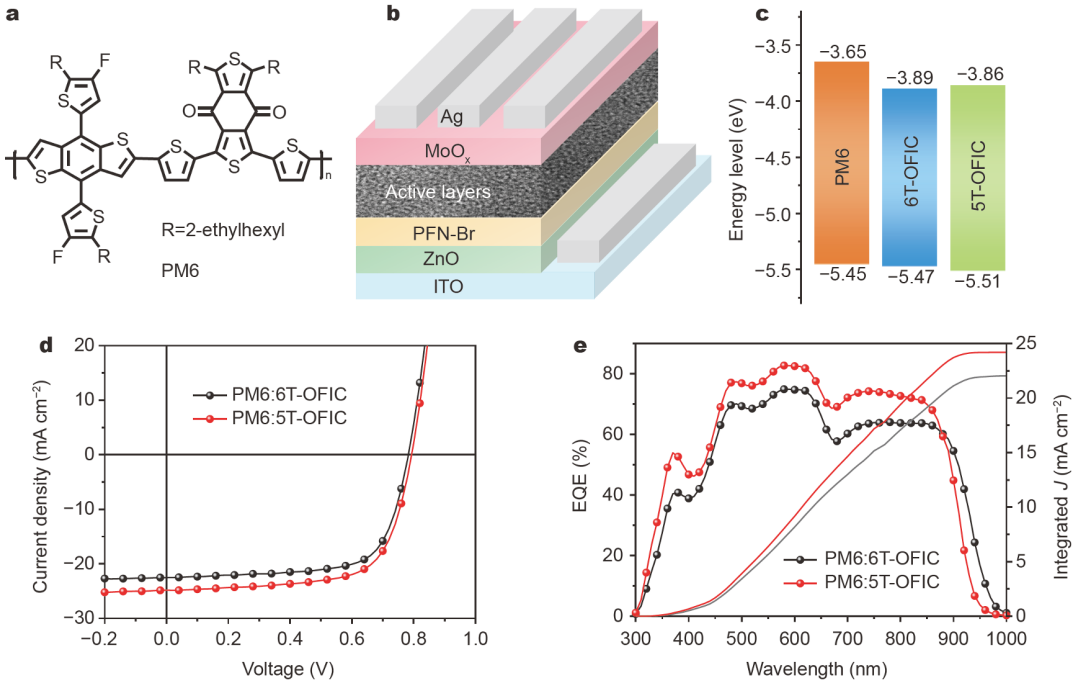

Figure 2 (a) Chemical structure of PM6. (b) Diagram of the inverted device structure. (c) Energy levels of the donor and acceptors. (d) *J*-*V* curves and (e) EQE spectra of the optimized PM6:6T-OFIC/5T-OFIC-based devices.

Table 2 The optimal photovoltaic parameters of PM6:6T-OFIC and PM6:5T-OFIC-based devices under AM 1.5 G Illumination (100 mW cm^{-2}) using the inverted device structures

Active layer	V_{oc} (V)	FF	J_{sc} (mA cm^{-2})	PCE (%)[a]
PM6:6T-OFIC	0.779±0.006 (0.782)	0.686±0.010 (0.696)	−22.50±0.441 (−22.69)	12.02±0.210 (12.35)
PM6:5T-OFIC	0.792±0.002 (0.794)	0.682±0.003 (0.681)	−24.32±0.277 (−24.84)	13.12±0.146 (13.43)

a) Statistical and optimal results are listed outside of parentheses and in parentheses, respectively. The average parameters were calculated from more than 10 devices.

transient photovoltage and photocurrent (TPV and TPC) decay kinetics of the 6T-OFIC- and 5T-OFIC-based devices. The 5T-OFIC-based device shows a shorter charge sweepout time of 0.25 μs than the 6T-OFIC-based device (0.36 μs). Moreover, the carrier lifetimes calculated from the TPV measurements are 47 and 84 μs for the 6T-OFIC- and 5T-OFIC-based devices, respectively. The shorter charge extraction time at short-circuit condition and higher lifetime of carriers at open-circuit voltage was correlated to the observed higher electron mobility and the weaker recombination in the 5T-OFIC-based devices. All these results contribute to improving the J_{sc} and keeping the high FF for the 5T-OFIC-based device to achieve its high performance.

The charge transport properties in the optimal PM6:6T-OFIC- and PM6:5T-OFIC-based devices were measured by the space-charge-limited current (SCLC) method using the hole-only or electron-only devices, respectively (Fig. S6). The calculated hole and electron mobilities for PM6:6T-OFIC and PM6:5T-OFIC are 2.62×10^{-4}, 3×10^{-4} cm^{-2} V^{-1} s^{-1} (μ_h), and 1.53×10^{-4}, 2.03×10^{-4} cm^{-2} V^{-1} s^{-1} (μ_e) with mobility ratios (μ_h/μ_e) of 1.71 and 1.48, respectively. Compared with the PM6:6T-OFIC-based device, the PM6:5T-OFIC-based device shows higher hole and electron mobility and more balanced μ_h/μ_e, which further supports its much higher J_{sc}.

Morphology characterization.

To characterize the morphology differences between the PM6:6T-OFIC blend film and PM6:5T-OFIC blend film, atomic force microscopy (AFM) and transmission electron microscopy (TEM) measurements were used. As displayed in Fig. 4a, b, the PM6:5T-OFIC film exhibits smaller and more finely dispersed phase separation with a root-mean-square surface roughness (R_q) of 2.78 nm compared with 3.42 nm of the PM6:6T-OFIC blend film.

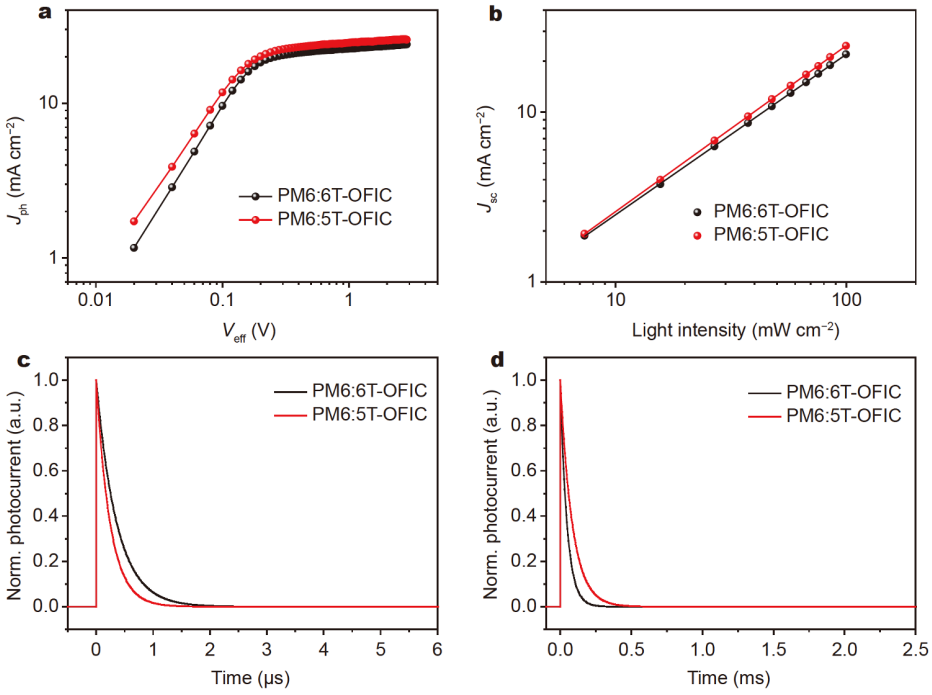

Figure 3 (a) J_{ph} *versus* V_{eff} and (b) light-intensity (P) dependence of J_{sc} for the optimized devices. (c) TPC and (d) TPV measurements of the PM6:6T-OFIC- and PM6:5T-OFIC-based devices.

Furthermore, in Fig. S7, the TEM image of the PM6:5T-OFIC blend film shows more continuous nanofiber-like networks. The distinctive morphologies for the PM6:5T-OFIC blend film are highly favorable for the charge generation and transport, which is in support of the above results [39].

To further investigate the impact of the molecular packing motifs and microstructure for these two acceptors, grazing incidence wide-angle X-ray scattering (GIWAXS) was investigated to characterize the neat film of 6T-OFIC and 5T-OFIC. As shown in Fig. S8, in the pristine film, PM6 pure film shows obvious face-on packing with a broad (100) diffraction peak around 0.29 Å^{-1} (d spacing: 22 Å) in the in-plane (IP) direction and a π-π stacking (010) diffraction around 1.70 Å^{-1} (d spacing: 3.69 Å) in the out-of-plane (OOP) direction, corresponding to the preferential face-on orientation. On the other hand, 6T-OFIC and 5T-OFIC all show relatively weak diffraction peaks with the introduction of alkyl chains in the backbones [36], indicating the relatively random molecular arrangement of the two neat films. However, after blending with the donor PM6, as depicted in Fig. 4c, d, the optimal binary blends of PM6:6T-OFIC and PM6:5T-OFIC display typical face-on orientation as PM6. In comparison with PM6, the two blend films exhibit enhanced and shifted (010) peaks at 1.76 Å^{-1} (d spacing: 3.57 Å) for the 6T-OFIC-based blend film and 1.75 Å^{-1} (d spacing: 3.59 Å) for the 5T-OFIC-based blend film, demonstrating that the optimized blend films lead to stronger π-π stacking. Moreover, compared with the PM6:6T-OFIC blend film, the PM6:5T-OFIC blend film shows a smaller crystal coherence length (CCL) (41.73 Å for 6T-OFIC and 31.84 Å for 5T-OFIC), estimated from the Scherrer equation. The smaller CCL indicates that the PM6:5T-OFIC-based blend is less inclined to aggregate than PM6:6T-OFIC, and results in proper phase separation, which is beneficial for charge transport in the OPV device, supporting the SCLC, AFM and TEM results [40].

Ternary blend devices.

Although the absorption edge of 5T-OFIC is close to the optimal one predicted by the model analysis, and the optimal J_{sc} is indeed as high as ~25 mA cm^{-2} and close to the predicted J_{sc} by the model analysis, the optimal PM6:5T-OFIC-based device still exhibits a relatively low V_{oc}, and unsatisfactory FF values compared with the desired values based on the model analysis. These make the overall performance of its device still significantly lower than the predicted performance. So, it is particularly needed to improve the corresponding V_{oc} and FF simultaneously. These results promote us to focus on the F-2Cl, which is one of our previously developed acceptor

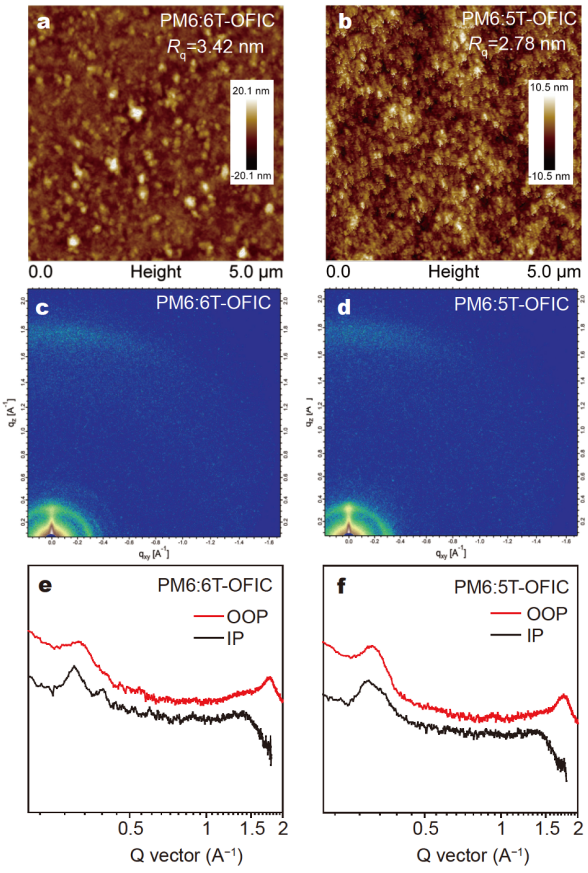

Figure 4 (a, c) AFM images and (b, d) GIWAXS for PM6:6T-OFIC and PM6:5T-OFIC. (e, f) IP and OOP line cuts of the GIWAXS patterns for PM6:6T-OFIC and PM6:5T-OFIC.

materials (Fig. S9a) [41]. Note this material has some very interesting and highly applicable characteristics here: 1) F-2Cl has a complementary absorption in the range of 650–790 nm (Figs S9b and S10), which is complementary with PM6 and 5T-OFIC. 2) More importantly, the PM6:F-2Cl-based device exhibits both a higher V_{oc} of 0.892 V and an outstanding FF of 0.78 [41]. Thus, it is expected that with the addition of F-2Cl, the ternary device PM6:F-2Cl:5T-OFIC might exhibit improved V_{oc} and FF. Indeed, after device optimization, a significantly improved PCE of 15.45% was achieved with a higher V_{oc} of 0.836 V, an enhanced J_{sc} of 25.46 mA cm^{-2} and a notably improved FF of 0.726 for the PM6:F-2Cl:5T-OFIC-based ternary device with a ratio of 1:0.6:0.4 (Table S4). Compared with the binary device of PM6:5T-OFIC, all the three parameters V_{oc}, J_{sc} and FF are improved simultaneously. The optimal *J*-*V* curve is presented in Fig. 5a and the corresponding parameters are summarized in Table S4. As shown in Fig. 5b, the ternary device exhibits an enhanced EQE response with the values over 80% in the region of 550–730 nm, indicating more efficient photoelectron conversion process in the ternary device [42–44]. The integrated photocurrent of PM6:F-2Cl:5T-OFIC from the EQE spectrum is 24.70 mA cm^{-2}, which is consistent with the J_{sc} value obtained from the *J*-*V* curve. In view of the above results, a molecular design strategy for synergetic enhancement of photovoltaic parameters was obtained. We believe that, through suitable material design and device optimization process, the PCEs of single-junction devices close to the theoretical calculation model (~20%) is around the corner.

CONCLUSION

In conclusion, we have designed and synthesized two new A-D-A type acceptors, 6T-OFIC and 5T-OFIC, under the guide of a semi-empirical model we proposed. Compared with 6T-OFIC, 5T-OFIC has a more suitable absorption range according to the semi-empirical model. After device optimization, the PM6:5T-OFIC-based device gives a PCE of 13.43%, which is higher than that of the PM6:6T-OFIC-based device (12.35%). To further improve its V_{oc} and FF, F-2Cl was used as the third component, the ternary device based on 5T-OFIC achieved a PCE of 15.45%, which is one of the highest performances so far

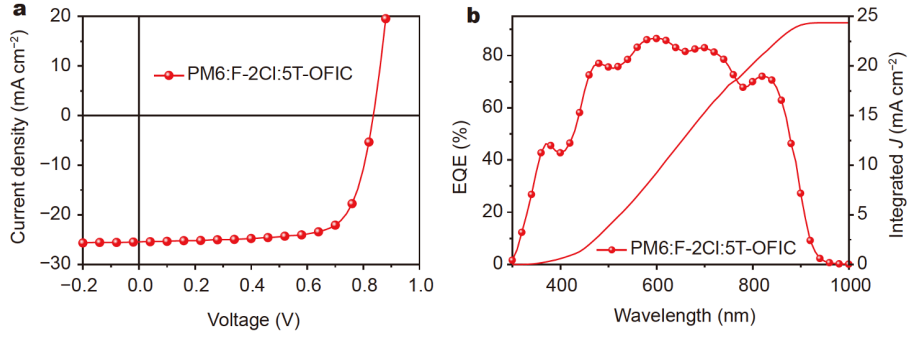

Figure 5 (a) *J*-*V* curve, (b) EQE spectrum of the optimized PM6:F-2Cl:5T-OFIC-based ternary devices.

except the Y6 series molecules. The results demonstrate that high-performance active layer materials can be designed following the semi-empirical model. With the variety of organic molecules, it is believed that higher-performance active layer materials can be designed and achieved in the near future to realize the commercialization of organic solar cells.

Received 10 December 2020; accepted 22 February 2021; published online 14 May 2021

1 Kim JY, Lee K, Coates NE, *et al.* Efficient tandem polymer solar cells fabricated by all-solution processing. Science, 2007, 317: 222–225
2 You J, Dou L, Yoshimura K, *et al.* A polymer tandem solar cell with 10.6% power conversion efficiency. Nat Commun, 2013, 4: 1446
3 Kan B, Li M, Zhang Q, *et al.* A series of simple oligomer-like small molecules based on oligothiophenes for solution-processed solar cells with high efficiency. J Am Chem Soc, 2015, 137: 3886–3893
4 Deng D, Zhang Y, Zhang J, *et al.* Fluorination-enabled optimal morphology leads to over 11% efficiency for inverted small-molecule organic solar cells. Nat Commun, 2016, 7: 13740
5 Xiao Z, Jia X, Ding L. Ternary organic solar cells offer 14% power conversion efficiency. Sci Bull, 2017, 62: 1562–1564
6 Bin H, Yang Y, Zhang ZG, *et al.* 9.73% efficiency nonfullerene all organic small molecule solar cells with absorption-complementary donor and acceptor. J Am Chem Soc, 2017, 139: 5085–5094
7 Chen Y, Wan X, Long G. High performance photovoltaic applications using solution-processed small molecules. Acc Chem Res, 2013, 46: 2645–2655
8 Hou J, Inganäs O, Friend RH, *et al.* Organic solar cells based on non-fullerene acceptors. Nat Mater, 2018, 17: 119–128
9 Cheng P, Li G, Zhan X, *et al.* Next-generation organic photovoltaics based on non-fullerene acceptors. Nat Photon, 2018, 12: 131–142
10 Meng L, Zhang Y, Wan X, *et al.* Organic and solution-processed tandem solar cells with 17.3% efficiency. Science, 2018, 361: 1094–1098
11 Yuan J, Zhang Y, Zhou L, *et al.* Single-junction organic solar cell with over 15% efficiency using fused-ring acceptor with electron-deficient core. Joule, 2019, 3: 1140–1151
12 Liu Q, Jiang Y, Jin K, *et al.* 18% efficiency organic solar cells. Sci Bull, 2020, 65: 272–275
13 Zhou Z, Xu S, Song J, *et al.* High-efficiency small-molecule ternary solar cells with a hierarchical morphology enabled by synergizing fullerene and non-fullerene acceptors. Nat Energy, 2018, 3: 952–959
14 Zhang G, Zhao J, Chow PCY, *et al.* Nonfullerene acceptor molecules for bulk heterojunction organic solar cells. Chem Rev, 2018, 118: 3447–3507
15 Wan X, Li C, Zhang M, *et al.* Acceptor–donor–acceptor type molecules for high performance organic photovoltaics–chemistry and mechanism. Chem Soc Rev, 2020, 49: 2828–2842
16 Sun H, Song X, Xie J, *et al.* PDI derivative through fine-tuning the molecular structure for fullerene-free organic solar cells. ACS Appl Mater Interfaces, 2017, 9: 29924–29931
17 Chen W, Zhang Q. Recent progress in non-fullerene small molecule acceptors in organic solar cells (OSCs). J Mater Chem C, 2017, 5: 1275–1302
18 Li G, Chang WH, Yang Y. Low-bandgap conjugated polymers enabling solution-processable tandem solar cells. Nat Rev Mater, 2017, 2: 17043
19 Sun Y, Chang M, Meng L, *et al.* Flexible organic photovoltaics based on water-processed silver nanowire electrodes. Nat Electron, 2019, 2: 513–520
20 Sun R, Wu Q, Guo J, *et al.* A layer-by-layer architecture for printable organic solar cells overcoming the scaling lag of module efficiency. Joule, 2020, 4: 407–419
21 Liu S, Yuan J, Deng W, *et al.* High-efficiency organic solar cells with low non-radiative recombination loss and low energetic disorder. Nat Photonics, 2020, 14: 300–305
22 Jiang K, Wei Q, Lai JYL, *et al.* Alkyl chain tuning of small molecule acceptors for efficient organic solar cells. Joule, 2019, 3: 3020–3033
23 Sun C, Qin S, Wang R, *et al.* High efficiency polymer solar cells with efficient hole transfer at zero highest occupied molecular orbital offset between methylated polymer donor and brominated acceptor. J Am Chem Soc, 2020, 142: 1465–1474
24 Lin Y, Adilbekova B, Firdaus Y, *et al.* 17% efficient organic solar cells based on liquid exfoliated WS_2 as a replacement for PEDOT:PSS. Adv Mater, 2019, 31: 1902965
25 Chao P, Chen H, Zhu Y, *et al.* A benzo[1,2-*b*:4,5-*c*′]dithiophene-4,8-dione-based polymer donor achieving an efficiency over 16%. Adv Mater, 2020, 32: 1907059
26 Zhou Z, Liu W, Zhou G, *et al.* Subtle molecular tailoring induces significant morphology optimization enabling over 16% efficiency organic solar cells with efficient charge generation. Adv Mater, 2019, 32: 1906324
27 Yan T, Song W, Huang J, *et al.* 16.67% rigid and 14.06% flexible organic solar cells enabled by ternary heterojunction strategy. Adv Mater, 2019, 31: 1902210
28 Li K, Wu Y, Tang Y, *et al.* Ternary blended fullerene-free polymer solar cells with 16.5% efficiency enabled with a higher-LUMO-level acceptor to improve film morphology. Adv Energy Mater, 2019, 9: 1901728
29 Sun H, Liu T, Yu J, *et al.* A monothiophene unit incorporating both fluoro and ester substitution enabling high-performance donor polymers for non-fullerene solar cells with 16.4% efficiency. Energy Environ Sci, 2019, 12: 3328–3337
30 Gao J, Wang J, An Q, *et al.* Over 16.7% efficiency of ternary organic photovoltaics by employing extra PC71BM as morphology regulator. Sci China Chem, 2019, 63: 83–91
31 Cui Y, Yao H, Zhang J, *et al.* Over 16% efficiency organic photovoltaic cells enabled by a chlorinated acceptor with increased open-circuit voltages. Nat Commun, 2019, 10: 2515
32 An Q, Wang J, Gao W, *et al.* Alloy-like ternary polymer solar cells with over 17.2% efficiency. Sci Bull, 2020, 65: 538–545
33 Luo Z, Sun R, Zhong C, *et al.* Altering alkyl-chains branching positions for boosting the performance of small-molecule acceptors for highly efficient nonfullerene organic solar cells. Sci China Chem, 2020, 63: 361–369
34 Ke X, Meng L, Wan X, *et al.* The rational and effective design of nonfullerene acceptors guided by a semi-empirical model for an organic solar cell with an efficiency over 15%. J Mater Chem A, 2020, 8: 9726–9732
35 Gao HH, Sun Y, Wan X, *et al.* Design and synthesis of low band gap non-fullerene acceptors for organic solar cells with impressively high j_{sc} over 21 mA cm^{-2}. Sci China Mater, 2017, 60: 819–828

36 Gao HH, Sun Y, Cai Y, *et al.* Achieving both enhanced voltage and current through fine-tuning molecular backbone and morphology control in organic solar cells. Adv Energy Mater, 2019, 9: 1901024
37 Zhang M, Guo X, Ma W, *et al.* A large-bandgap conjugated polymer for versatile photovoltaic applications with high performance. Adv Mater, 2015, 27: 4655–4660
38 Blom P , Mihailetchi V , Koster L , *et al.* Device physics of polymer: Fullerene bulk heterojunction solar cells. Adv Mater, 2007, 19: 1551–1566
39 Huang Y, Kramer EJ, Heeger AJ, *et al.* Bulk heterojunction solar cells: Morphology and performance relationships. Chem Rev, 2014, 114: 7006–7043
40 Liu T, Zhang Y, Shao Y, *et al.* Asymmetric acceptors with fluorine and chlorine substitution for organic solar cells toward 16.83% efficiency. Adv Funct Mater, 2020, 30: 2000456
41 Zhang Y, Feng H, Meng L, *et al.* High performance thick-film nonfullerene organic solar cells with efficiency over 10% and active layer thickness of 600 nm. Adv Energy Mater, 2019, 9: 1902688
42 Lu L, Kelly MA, You W, *et al.* Status and prospects for ternary organic photovoltaics. Nat Photon, 2015, 9: 491–500
43 Gasparini N, Jiao X, Heumueller T, *et al.* Designing ternary blend bulk heterojunction solar cells with reduced carrier recombination and a fill factor of 77%. Nat Energy, 2016, 1: 16118
44 Liu T, Luo Z, Chen Y, *et al.* A nonfullerene acceptor with a 1000 nm absorption edge enables ternary organic solar cells with improved optical and morphological properties and efficiencies over 15%. Energy Environ Sci, 2019, 12: 2529–2536

Acknowledgements The work was supported by the Ministry of Science and Technology, China (2019YFA0705900 and 2016YFA0200200), the National Natural Science Foundation of China (21935007, 52025033 and 51773095), Natural Science Foundation of Tianjin (20JCZDJC00740 and 17JCJQJC44500) and the 111 Project (B12015).

Author contributions Meng L, Chen Y, Gao HH and Wu S designed the project; Wan X, Li C and Chen Y directed the research; Meng L, Sun Y, Guo Z and Chen H fabricated and characterized the devices. Yang Y and Wang J performed the GIWAXS measurements. Meng L wrote the paper, with support from Chen Y. All authors contributed to the general discussion.

Conflict of interest The authors declare no conflict of interest.

Supplementary information Experimental details and supporting data are available in the online version of the paper.

Lingxian Meng is a PhD candidate under the supervision of Profs Yongsheng Chen and Xiangjian Wan at Nankai University. She received her Bachelor degree from the College of Chemistry and Molecular Engineering, Zhengzhou University in 2016. Her research focuses on organic photovoltaic materials.

Huan-Huan Gao is a PhD candidate under the supervision of Profs Yongsheng Chen and Xiangjian Wan at Nankai University. She received her BSc degree in chemistry from Nanyang Normal University in 2013 and MSc degree in organic chemistry from Nankai University in 2016. Her research focuses on the design and synthesis of organic photovoltaic materials.

Simin Wu is a Master candidate under the supervision of Prof. Yongsheng Chen at Nankai University. He received his BSc degree in polymer materials and engineering from Beijing University of Chemical Technology in 2019. His research focuses on the design and synthesis of organic photovoltaic materials.

Yongsheng Chen received his PhD in chemistry from the University of Victoria in 1997. From 2003, he has been a Chair Professor at Nankai University. His main research interests focus on carbon-based nanomaterials and organic functional materials for green energy applications.

半经验模型指导受体分子结构优化获得效率超过15%的有机太阳能电池

孟令贤[1†], 高欢欢[1†], 吴思敏[1†], 孙延娜[1], 万相见[1], 杨扬[2], 王剑[2], 郭子琦[1], 陈红滨[1], 李晨曦[1], 陈永胜[1*]

摘要 本工作中, 在我们发展的半经验模型的指导下, 设计合成了两个A-D-A骨架受体分子, 6T-OFIC和5T-OFIC. 因其较长的共轭骨架, 6T-OFIC的截止吸收波长为946 nm. 相比于6T-OFIC, 因其骨架少一个噻吩单元, 5T-OFIC分子的截止吸收波长为927 nm, 更接近半经验模型所预测的最佳单结器件的截止吸收波长. 最终, 基于PM6:5T-OFIC的器件获得了13.43%的能量转换效率, 高于PM6:6T-OFIC器件. 以F-2Cl作为第三组份, 基于PM6:F-2Cl:5T-OFIC的三元器件其填充和开压得到了明显的提高, 最终获得了15.45%的能量转换效率.